ACS OMEGA

http://pubs.acs.org/journal/acsodf

Article

Protecting Light Metal Alloys Using a Sustainable Plasma Electrolytic Oxidation Process

Fengyan Hou, Rukmini Gorthy,* Ian Mardon, Da Tang, and Chris Goode

Cite This: *ACS Omega* 2022, 7, 8570−8580

Read Online

ACCESS | Metrics & More | Article Recommendations

ABSTRACT: Low-density metals such as Mg and Al (and their alloys) are of high interest for lightweight engineering applications in various industries. Moisture sensitivity, poor tribology, and corrosion susceptibility limit the direct application of these light metals. Plasma electrolytic oxidation (PEO) is extensively used to passivate light metals against corrosion and enhance their mechanical properties. PEO processes in current use are often energy-intensive and use toxic electrolytes. Incorporating composite characteristics to PEO-treated surfaces typically requires modification of electrolytes with nanoparticle addition. Some applications also need post-treatment of oxidized coatings to ensure functionality. We report a versatile, environmentally friendly PEO process that uses organo-silicate electrolytes enriched with nitrogen-containing solutions. The single-step process produces ∼6 μm thick, uniform, adherent, and porous oxide coatings on AZ80 and Al6061 surfaces in 15 min. We evaluated the influence and effectiveness of in situ nitridation by comparing the coating properties with those on alloys treated in PEO electrolytes without nitrogen-containing chemicals. The two sets of coatings were porous with multilayered basalt-like topographies and were composed of metal oxides and metal silicates. Alloys treated in nitrogen-containing electrolytes exhibited the presence of oxynitrides. The use of nitrogen-containing PEO electrolytes resulted in coatings with enhanced mechanical behavior. We found that the corrosion resistance of coatings prepared using low voltages in this study was comparable to the traditional PEO-treated coatings reported in the literature. Nitridation of the coatings, however, appears to have a slightly negative influence on the coatings' corrosion resistance. Our future work will focus on improving the corrosion resistance of the mechanically resilient, nitride-containing PEO-treated coatings.

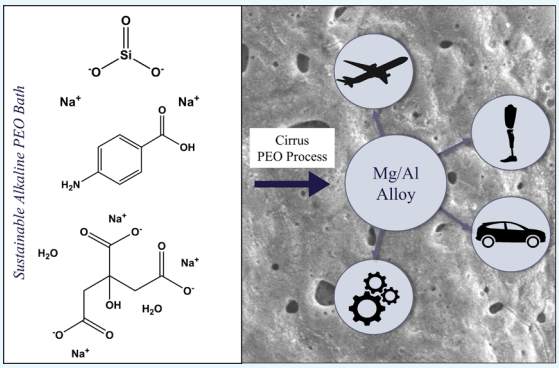

INTRODUCTION

Magnesium and aluminum alloys are of high interest for lightweight engineering and design applications in automotive, electronics, computer, and sporting goods industries.[1] Wear and corrosion susceptibility of Mg and Al alloys limit their direct applicability. Surface modification techniques such as physical vapor deposition (PVD), chemical vapor deposition (CVD), sol−gel coating, chemical conversion coating, electroplating, thermal spraying, and anodizing are commonly employed to protect light metals. Wu et al. used PVD to produce corrosion-resistant oxynitride-based coatings on Mg alloys. The authors report that the incorporation of AlO_XN_Y into the protective coatings enhanced the bio-corrosion resistance of Mg in simulated physiological environments.[2] Liu et al. reported the enhanced tribological behavior of Al7075 when coated with TiAlN via PVD.[3] Noder et al. published their findings reporting the improved tribological behavior of PVD-coated Al alloys machined for automotive structural components.[4] Ishizaki et al. reported the use of CVD to protect Mg alloys (AZ321) from corrosion by inducing superhydrophobic characteristics to the surface. The authors also report the high chemical stability of the CVD coatings in acidic, neutral, and alkaline environments.[5] The drawback of using PVD and CVD techniques for light metal protection is the incompatibility of the mostly ceramic coatings with the metallic substrates. Gadow et al. reported that coatings prepared by PVD and/or CVD processes often exhibit low elasticity and thus are susceptible to mechanical damage.[6] Economic feasibility and process scalability led to the wide use of sol−gel for protective coatings on light metals. Shadanbaz and Dias reported the synthesis of calcium phosphate coating using a sol−gel technique on biocompatible Mg substrates. The study reported some ways in which calcium phosphate coatings impeded the corrosion rates of Mg-based bone implants.[7] Other reviews by Wang et al. and Vazirinasab et al. reported the synthesis of superhydrophobic coatings by the

Received: November 15, 2021
Accepted: February 2, 2022
Published: March 2, 2022

https://doi.org/10.1021/acsomega.1c06442
ACS Omega 2022, 7, 8570−8580

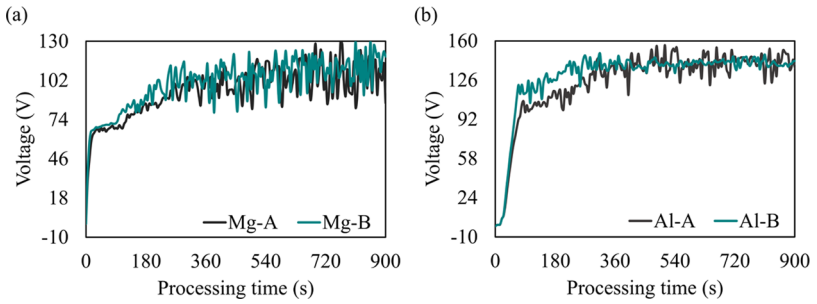

Figure 1. Voltage vs time graphs showing the low energies required to produce oxide coatings on (a) Mg AZ80 alloys and (b) Al6061 alloys with and without nitrogen-containing PEO electrolytes.

sol−gel process on Mg and Al alloys to improve the substrates' corrosion resistance.[8,9] The negative aspect of using sol−gel coatings is their poor adherence to metallic substrates. Chemical conversion is another common process used to generate adherent coatings on light metal substrates. Chemical or electrochemical reactions between substrates and highly toxic chromate-based treatments form conversion coatings. Some less toxic alternates for conversion coatings on Mg alloys are phosphate- and/or stannate-based solutions.[10] Becker reviewed Zr/Ti-based chemical conversion coatings to protect Al alloys for applications in aeronautics industries.[11] While conversion coatings are more adherent to Mg/Al alloy surfaces, they are prone to cracking, thereby reducing their efficacy as corrosion protectors.[12] Electroplating is one of the oldest techniques employed to protect metallic substrates from corrosion; however, most aqueous electroplating solutions are not suitable for self-passivating (Mg or similar) alloys. Self-passivating coatings are nonuniform and interfere with the adhesion of electrodeposited coatings.[13] Gu et al. electro-deposited nanocrystalline Ni coatings on AZ91D substrates to enhance their corrosion resistance. The authors employed an electroless Ni conversion coating to mitigate the passivation of Mg in aqueous plating baths.[14] Abbott et al. reviewed the utilization of ionic liquids as plating baths for protecting Mg and Al alloys from corrosion. The authors note that environmental compatibility is not a natural consequence of using ionic liquids for electroplating.[15]

Plasma electrolytic oxidation (PEO) or micro-arc oxidation (MAO) is a well-known surface treatment process for protecting light metallic materials such as Be, Mg, Al, and Ti.[16] Markov et al.[17,18] introduced the original notion of generating oxidized coatings on metals using discharge energy. Traditional PEO processes are energy-intensive. PEO occurs by applying high voltages between a target electrode and a stable cathode via direct current (DC), pulsed DC, or alternating current (AC) in an electrolyte. The high voltages generate a plasma state localized at the arc discharge points, leading to the formation of adherent mixed oxide coatings on the metallic substrates. The bidirectional coating growth takes place by the formation of a porous surface layer and extending into the bulk of the substrate. The coatings exhibit a range of desirable properties such as strong adhesion, high hardness, thermal and electrical insulation, and high corrosion resistance.

Factors such as processing voltages, current density, temperature, and electrolyte composition influence the performance of PEO-treated surfaces. The chemical composition of a PEO electrolyte plays a significant role in the formation and performance of coatings.[19] For example, enhanced hardness of PEO-treated surfaces can be attributed to silicate and phosphate compounds in electrolytes.[20,21] Other studies on the enhancement of the coatings' performance entailed the incorporation of secondary substances during PEO treatments. Pezzato et al. used molybdate salts in an alkaline PEO electrolyte to treat Mg alloys and improve their corrosion resistance.[22] Lee et al. added CNTs to PEO electrolytes to enhance the densification of resulting coatings on Al alloys.[23] Studies are also available on the incorporation of carbide and nitride content into PEO-treated coatings by adding materials such as WC and TiN nanoparticles to the electrolytes.[19,24]

Cirrus Materials aimed to design a sustainable PEO process for light metal surface modification in the current study. Here, we report a PEO surface modification process that produces adherent and mechanically robust coatings on Mg and Al alloys using low-energy and benign silicate-based organo-alkaline electrolytes. Approaches to simultaneous nitridation and carburization of the coatings entailed the addition of nitrogen-containing eco-friendly organic chemicals to the PEO electrolytes. The resulting coatings were composites of metal oxides, oxynitrides, carbonates, and silicates. Our primary target was to devise a single-step method to produce protective ceramic coatings on Mg and Al alloys enhanced with silicate and nitrogen-containing compounds. We use commonly available chemicals. The PEO baths are very stable at the laboratory level and do not require replenishment. However, at an industrial scale, we expect bath maintenance to be a process cost. Once prepared, the baths can be safely stored at room temperature. This is a very cost-effective feature of our technology. Additionally, the total energy consumed for treating Mg or Al using this technology is less than 35 W-h/dm^2, making it a sustainable surface treatment process. We have evaluated the energy contribution of both the PEO energy and process energy and determined that compared to the traditional PEO, the consumption is less than 10%.

RESULTS AND DISCUSSION

Synthesis. We used a single-electrolyte formulation to create PEO surfaces on Mg-A and Al-A alloys. We modified the same bath using an aminophenolic compound to treat samples Mg-B and Al-B. The aminophenol modification of bath chemistry was a pathway to incorporate nitride content into the coatings to enhance their mechanical behavior. The samples treated in PEO baths with and without aminophenols have similar appearance. Figure 1 shows the variation of voltage during PEO treatment of AZ80 and Al6061 alloys. The graphs show the low processing voltages required to form oxide layers on the Mg and Al alloy surfaces. The processing voltage for AZ80 alloys is <130 V (Figure 1 a), and that for Al6061 alloys is <160 V (Figure 1 b). These values are lower

https://doi.org/10.1021/acsomega.1c06442
ACS Omega 2022, 7, 8570−8580

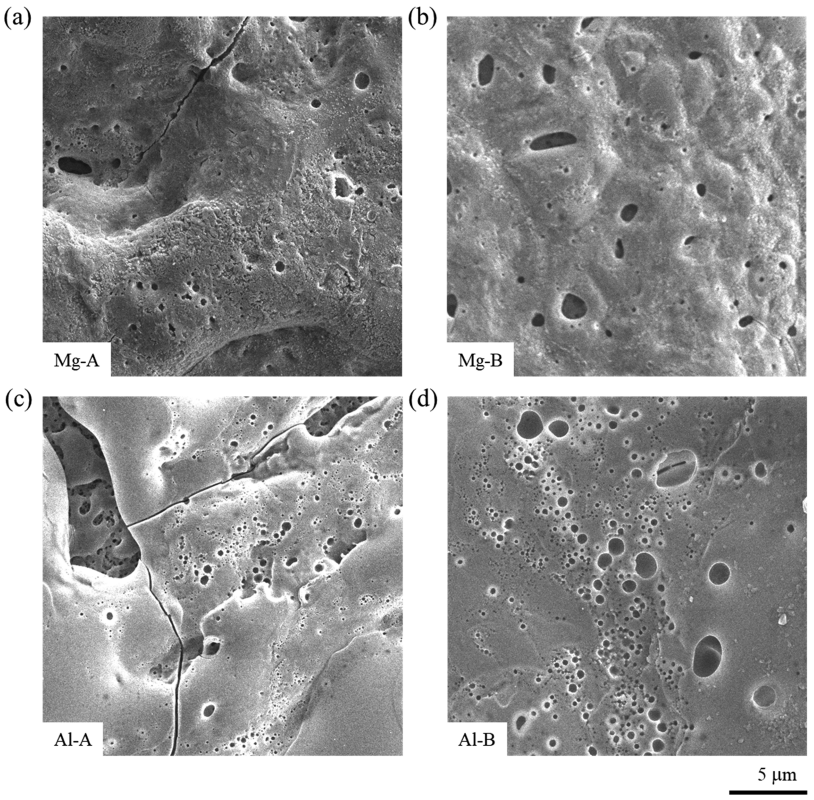

Figure 2. (a) Surface morphology of Mg-A. The porous oxide layer on AZ80 alloy treated in PEO bath is shown. The cracks and varied pore dimensions are typical of a surface treated using PEO. (b) Surface morphology of Mg-B. The morphology appears flatter and more uniform compared to Mg-A coatings. We also see an improved uniformity in the pore distribution for Mg-B surfaces. (c) Surface morphology of Al-A. The porous oxide layer formed because the PEO surface treatment of Al6061 alloys shows a nonuniform morphology with prominent surface cracks. (d) Surface morphology of Al-B. Treating Al6061 alloys with nitrogen-containing PEO bath altered the appearance of the resultant porous oxide coating. The pore dimensions are larger on the Al-B surface, and there are no prominent cracks.

than the ca. 400−700 V typically used in traditional PEO processes.[25−27] In the case of Mg, low current densities are sufficient to generate surface arcs required to produce the oxide coating. The use of high current densities tends to burn the Mg oxide coating. Using the same current density on Al would produce a lower arc density, thus requiring a longer duration to breach the barrier layer and generate a coating. Also, Al can be processed at high current densities without burning the coatings. Thus, we selected 1 A/dm^2 for Mg and 4 A/dm^2 for Al.

There are some reported studies on using either low PEO processing voltages or nontoxic electrolytic chemicals. However, we found little research on the combination of low processing voltages and benign electrolytic chemicals for PEO surface treatment. Cai et al. report using an ∼140 V processing voltage in a relatively toxic bath for surface treating AZ91D Mg alloys and incorporated cerium oxide into the surface oxide layer during the micro-arc oxidation (MAO) treatment to enhance the mechanical properties of the coating.[28] Dong et al. have also reported using a low-voltage MAO process to produce oxide film on AM60 Mg alloy in fluoride-based electrolytic baths.[29] The lowest processing voltage reported for aluminum alloys is in the range of 350−500 V. Lee et al. used a 375 V processing voltage to produce an oxide layer on Al7075 alloy surfaces.[23] Zhang et al. prepared PEO coatings on pure aluminum at an ∼500 V processing voltage and using varying current densities.[30] Compared to the studies presented by other research groups, the PEO treatment process reported in this paper is significantly less energy-intensive and uses environmentally friendly electrolytes.

Surface Morphology. Macroscopically, Mg and Al alloys treated in PEO electrolytes with and without nitrogen-containing compounds possess a similar appearance. Scanning electron microscope (SEM) images (Figure 2) of the surface-treated alloys showed that the addition of aminophenols to the PEO electrolyte has significantly changed the surface morphologies of the coatings. Mg-A and Al-A, PEO-treated in an organo-silicate electrolyte, exhibit pores and surface cracks typical of the ceramic oxide coating.[26] Mg-A coating (Figure 2a) exhibits plateau-like features and pores of varying dimensions. The surface cracks appear to propagate into the coating by a few nanometers. Mg-B coatings (Figure 2b) exhibit a basalt-like morphology with uniformly distributed pores on the surface. The pore dimensions range from 10 nm to around 2.00 μm. Al-A coating (Figure 2c) shows sporadically distributed pores of <50 nm and a bilayer surface morphology. The coating also exhibits surface cracks on the surface that appear to propagate in the coating. Al-B coatings (Figure 2d) show increased porosity and a spongelike morphology. The average pore dimensions are larger compared to Al-A and range from 10 nm to ∼1.5 μm. We do not see any prominent cracks on Al-B. The observed uniformities in surface morphologies of Mg-B and Al-B suggest the presence of an aminophenol in PEO electrolytes supplying diffusion pathways for an even distribution of generated arc energies.

https://doi.org/10.1021/acsomega.1c06442
ACS Omega 2022, 7, 8570−8580

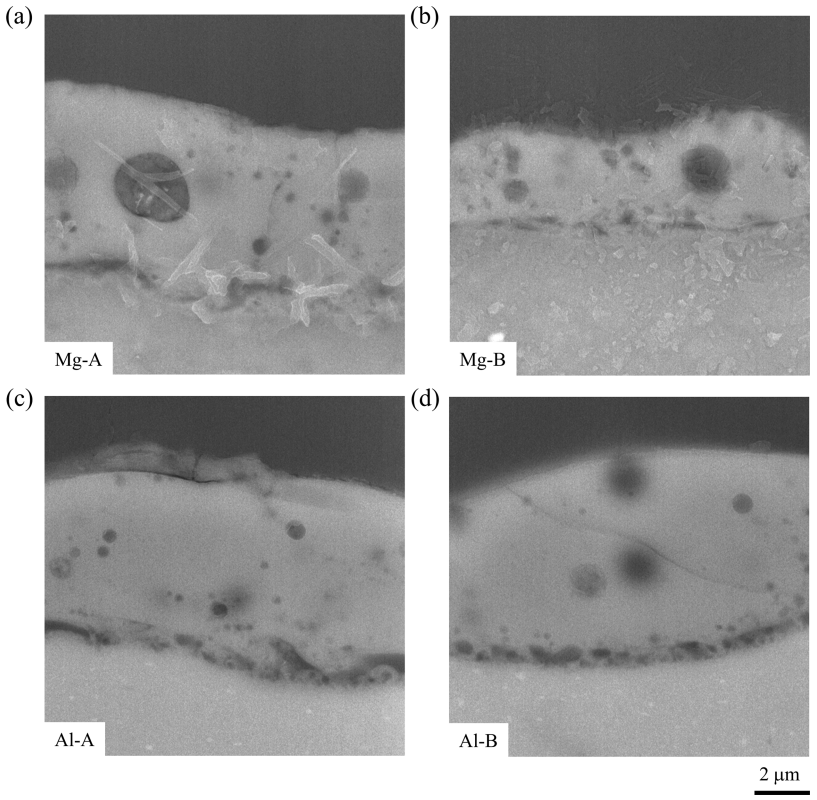

Figure 3. Cross-sectional morphologies of (a) Mg-A coating on PEO-treated AZ80 alloy, (b) Mg-B coating on PEO-treated AZ80 alloy with a nitrogen-containing compound in the electrolytic bath, (c) Al-A coating on PEO-treated Al6061 alloy, and (d) Al-B coating on Al6061 alloy treated in nitrogen-containing PEO electrolyte.

The cross sections (Figure 3) of the PEO-treated Mg and Al alloys analyzed using SEM showed interesting variations. Mg-A coating, in Figure 3a, is 6 μm thick and exhibits nonuniform porosity with an ∼20 nm thick barrier layer between the coating and the alloy. The image illustrates that the surface cracks observed in Figure 2a extend the entire depth of the film and propagate through the pores. PEO treatment of Mg alloys in the nitrogen-containing electrolyte produces a thinner oxide coating. The coating (Figure 3b) is ∼3.5 μm thick and porous. Mg-B does not exhibit any cracks, suggesting that the coating could produce superior mechanical behavior compared to Mg-A. We also observe that the barrier layer between the Mg-B coating and the substrate is thinner than that of Mg-A. It is possible that the difference in the coating thickness could influence the mechanical performance of the coating and affect the corrosion protection properties. The coatings on aluminum alloys (Figure 3c,d) are both ∼6 μm thick but exhibit different porous characteristics. Figure 3c confirms that Al-A coating possesses a trilayer morphology with pores distributed sporadically through the depth of the coating. The surface cracks (Figure 2c) appear only in the top layer. The image also shows the presence of a barrier layer between the aluminum oxide coating and the Al6061 alloy. The layer appears to be ∼50 nm thick and nonuniform along the coating−substrate interface. Al-B coating (Figure 3d) does not exhibit the surface layer seen in Al-A. The figure also shows that the cross-sectional porosity of aluminum alloys treated in nitrogen-containing PEO baths is different from the porosity observed on the surface (Figure 2d) of the coating. We observe cracks in the Al-B coating that are not evident from SEM images. The interfacial layer between the Al-B coating and substrate is more uniform compared to the Al-A and substrate. Our hypothesis is that the improved uniformity is due to the presence of nitrogen-containing polymeric compounds in the PEO baths. Epoxy contamination during sample preparation obscures the porosity.

PEO-produced micro-plasma, at localized discharge points, creates high thermal and pneumatic energies at the alloy−electrolyte interface. The high thermal energies both melt the substrate and ionize the electrolyte surrounding the arc discharge point. The pressure variation between the generated plasma and molten substrate surface causes gases from the substrate bulk to bubble to the surface, while silicates and oxides are diffused into the surface developing a porous crystalline oxide composite coating.[31] The highly porous interfacial layer between the coating and the substrate is a characteristic property of PEO-treated surfaces.[32] The addition of a nitrogen-containing polymer to the PEO bath appears to suitably distribute the energy fluxes along the substrate surface, which could explain the high degree of uniformity observed on Mg-B and Al-B coatings.

Composition. *Crystallographic Analysis.* Figure 4 shows the X-ray diffraction (XRD) patterns collected for the PEO-treated AZ80 and Al6061 alloys. The insets are at a higher graphical magnification to highlight the low-intensity peaks, which are not obvious from the overall spectra. The Mg alloy surfaces exhibited different compositions and crystallographic signatures for the samples treated in PEO baths with and without nitrogen-containing compounds. Mg-A coating (Figure 4a) is composed of oxides, hydroxides, and silicates of magnesium. The XRD patterns also show the presence of alumina and silica in the Mg-A coating. Additionally, we

https://doi.org/10.1021/acsomega.1c06442
ACS Omega 2022, 7, 8570−8580

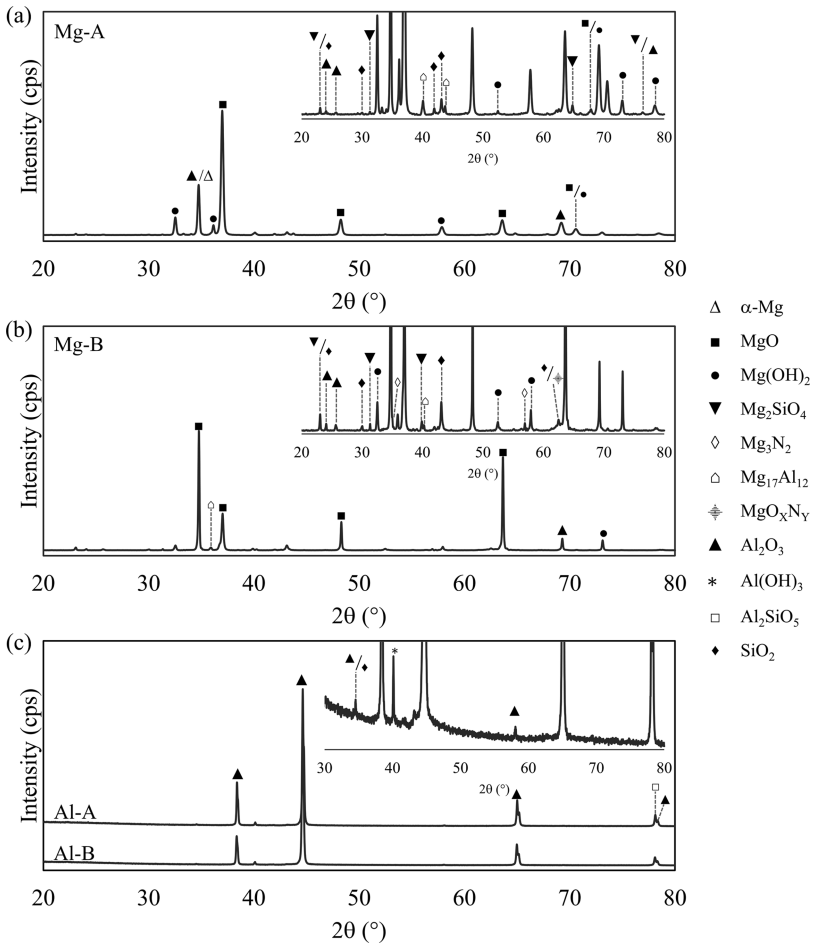

Figure 4. XRD patterns for PEO-treated AZ80 and Al6061 alloys. (a) Mg-A coatings on AZ80 alloys prepared in PEO electrolyte without nitrogen-containing polymers. The pattern shows the presence of Mg, Mg-Al, MgO, and magnesium silicates. (b) Mg-B coatings on AZ80 alloys prepared in aminophenol-containing PEO bath. The pattern exhibits the presence of all of the compounds detected in Mg-A along with nitrides of Mg. (c) Al-A and Al-B coatings exhibit similar crystallographic composition consisting of aluminum oxides and silicates.

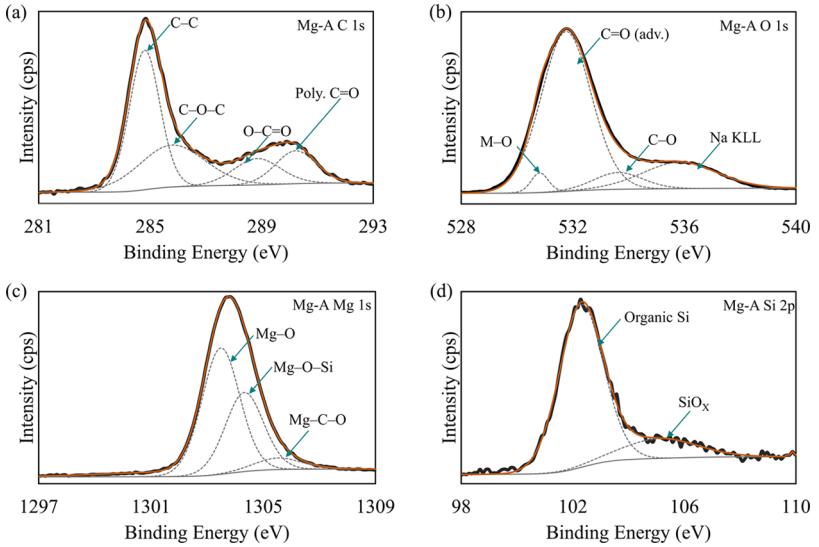

Figure 5. XPS core-level scans for Mg-A coatings. (a) Spectrum showing deconvoluted C 1s peaks with C−C aligned at 284.8 eV; (b) deconvoluted spectrum for O 1s at ∼530 eV; (c) deconvoluted spectrum for Mg 1s at ∼1303 eV; and (d) deconvoluted spectrum for Si 2p at ∼102 eV.

detected the presence of α-Mg and magnesium aluminide ($Mg_{17}Al_{12}$) in the Mg-A coating composition. The highest intensity peaks in Mg-A XRD suggest that MgO dominates the crystallographic signature of the coatings. The intensities of

https://doi.org/10.1021/acsomega.1c06442
ACS Omega 2022, 7, 8570−8580

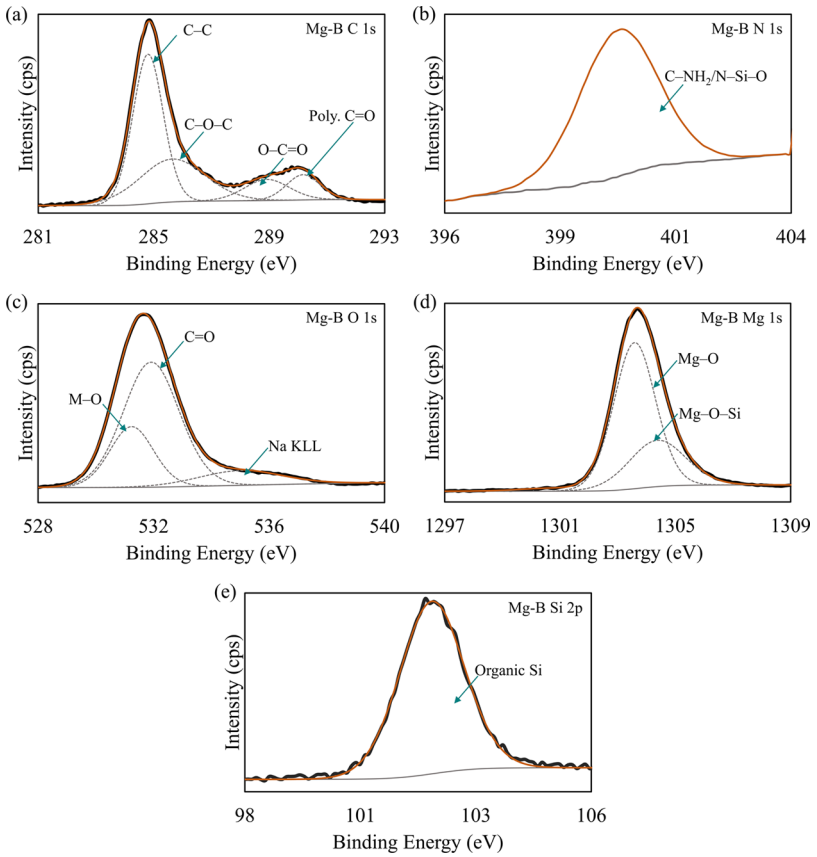

Figure 6. XPS core-level scans for Mg-B coating on AZ80 alloy. (a) Deconvoluted C 1s spectrum with C−C peak aligned at 284.8 eV; (b) N 1s spectrum at ∼399 eV; (c) deconvoluted O 1s spectrum at ∼533 eV; (d) deconvoluted Mg 1s spectrum at ∼1303 eV; and (e) spectrum for Si 2p at ∼102 eV.

peaks at 2θ = 32.52° and 2θ = 34.74° indicate that Al_2O_3 and $Mg(OH)_2$ also influence the degree of crystallinity of Mg-A coatings but to a lesser extent than MgO. The XRD pattern of Mg-B (Figure 4b) shows the presence of oxides, hydroxides, and silicates of Mg; oxides of aluminum; and oxides of silicon in the coatings. The patterns also indicate the presence of Mg_3N_2 and MgO_XN_Y in the coating. The peak intensities corresponding to MgO appear to be higher and sharper for Mg-B coatings even at higher 2θ values (48.3 and 63.7°). These results suggest that the addition of nitrogen-containing compounds to the bath chemistry improved the degree of crystallinity of magnesium oxide in the coating. We hypothesize that the arc energies generated during amino-phenol-enhanced PEO treatment of AZ80 alloys are sufficiently high for the formation of Mg_3N_2 in the coating chemistry.[33] The appearance of magnesium oxynitride in the coating chemistry could suggest that the localized arc energies are capable of nitriding MgO.

The XRD patterns of Al-A and Al-B coatings (Figure 4c) both exhibited similar crystallographic signatures. Al-A and Al-B coatings are composed of alumina, aluminum hydroxide, and aluminum silicates. From the XRD peak intensities for Al-A and Al-B coatings, we observe that alumina exhibits the highest degree of crystallinity. The peak at 2θ = 24.2° is higher for Al-A compared to Al-B coatings. The results for PEO-treated Al6061 alloys indicate that nitrogen-containing electrolytic bath does not significantly influence the crystallographic composition of the Al-based oxide layers.

Surface Chemistry. We obtained a detailed analysis of the surface compositions on the PEO-treated Mg and Al alloys using X-ray photoelectron spectroscopy (XPS). The results determine the binding states of various elements in the composite coatings. Figure 5 shows the core-level spectra collected from the surface of Mg-A coating. C 1s spectral (Figure 5 a) deconvolution resulted in three distinct binding states of carbon for the PEO-treated surface. Accumulated adventitious carbon is responsible for the C−C peak at 284.8 eV, C−O−C peak at 285.8 eV, and O−C═O at ∼289 eV. The C−O−C signature due to the carbonate content in the coating is indistinguishable from adventitious contamination. The spectrum also indicates the presence of some polymeric carbon at 290.2 eV, assumed to be the result of citrates in the PEO bath chemistry. There are no observed metal−carbon bonds from the deconvoluted C 1s spectrum. Figure 5b shows the deconvoluted O 1s spectrum for Mg-A coating. The peaks at 532 and 533.2 eV are the signals from C−O bonds of the adventitious carbon content. The peak at 530.9 eV is from the metal oxide content of the coating. We also observe the Na auger peak at ∼536 eV. We attribute the presence of sodium in the coating to remnant contamination from the PEO electrolyte. Figure 5c provides the peak deconvolution for the Mg 1s spectrum. Mg 1s constituent peaks indicate the presence of MgO (1303.5 eV)[34] and magnesium silicates (1304.3 eV)[35] in Mg-A coating. The peak at 1305.5 eV indicates the presence of $MgCO_3$. The spectral deconvolution of Si 2p resulted in two peaks. The majority of the signature is

https://doi.org/10.1021/acsomega.1c06442
ACS Omega 2022, 7, 8570−8580

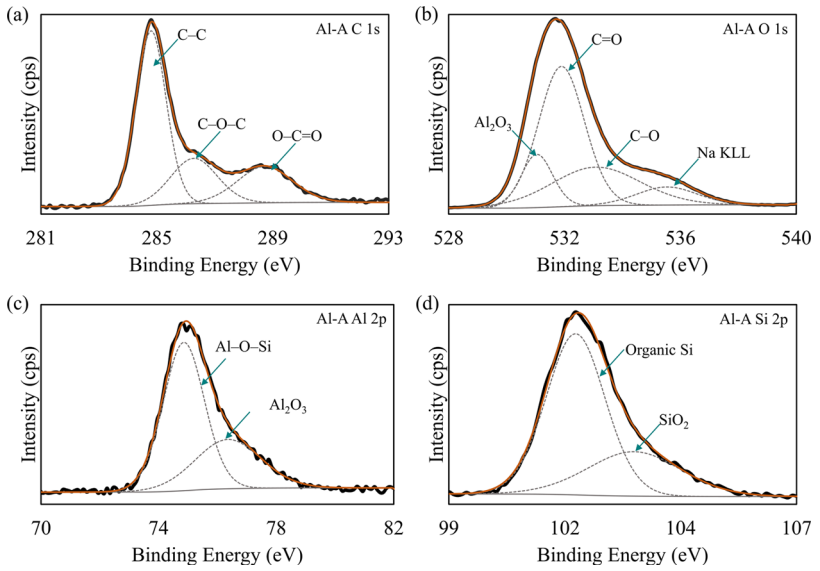

Figure 7. Al-A core-level scans obtained from XPS. (a) Deconvoluted C 1s spectrum with C−C peak aligned at 284.8 eV; (b) deconvoluted O 1s spectrum at ∼533 eV; (c) deconvoluted Al 2p spectrum at ∼74 eV; and (d) deconvoluted Si 2p peaks at ∼102 eV.

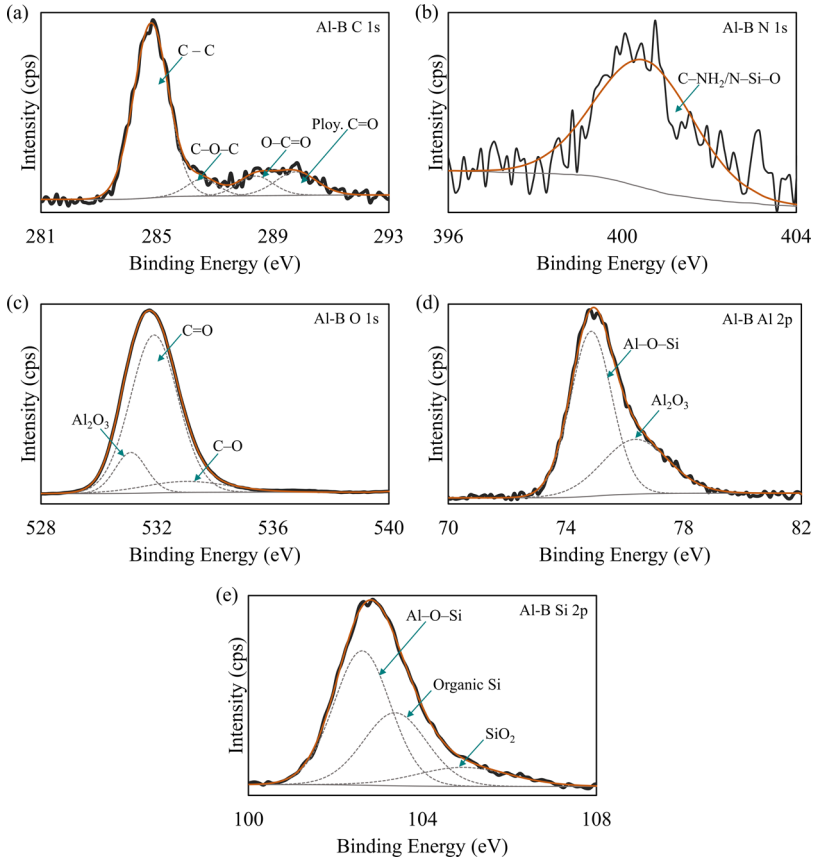

Figure 8. Al-B core-level scans obtained from XPS. (a) Deconvoluted C 1s spectrum with a C−C peak aligned at 284.8 eV; (b) an N 1s spectral peak at ∼399 eV; (c) a deconvoluted O 1s spectrum at ∼533 eV; (d) a deconvoluted Al 2p spectrum at ∼74 eV; and (e) a deconvoluted Si 2p peak at ∼102 eV.

due to organic silicon (102.3 eV) content in Mg-A. The peak at 105.1 eV corresponds to Si−O bonds in the coating.

Figure 6 provides the core-level spectra collected for C, N, O, Mg, and Si content in Mg-B coatings. The results show that the binding states for C, O, Mg, and Si elements in Mg-B coatings are almost identical to their counterparts in Mg-A coatings. The spectra were analyzed by aligning the C−C peak in the C 1s spectrum at 284.8 eV. The N 1s peak at ∼400 eV (Figure 6c) indicates overlapping signatures from C−NH_2 bonds and silicon oxynitrides in the coating. The Mg 1s peak deconvolution (Figure 6d) shows that we did not detect any signature from magnesium carbonates in Mg-B coatings. This

https://doi.org/10.1021/acsomega.1c06442
ACS Omega 2022, 7, 8570−8580

result only indicates that $MgCO_3$ might not be present in the top ~20 nm of the coating formed by aminophenol-enhanced PEO treatment. The Si 2p signature at 102.3 eV (Figure 6e) on the surface is from the organic silicon content.

Figure 7 illustrates the XPS core-level spectra collected for Al-A coatings. The C 1s peak deconvolution, seen in Figure 7a, exhibits the presence of C−C bonds aligned at 284.8 eV, C−O−C bonds at 286.3 eV, and O−C═O bonds at 288.7 eV. The carbon signature is primarily due to adventitious carbon accumulated on the coating surface. The O−C═O peak suggests the presence of carbonyl and carboxyl functional groups in the coating. However, these are indistinguishable from the accumulated adventitious carbon. The O 1s peak deconvolution (Figure 7b) indicates that the coating contains Al_2O_3 (531.1 eV), C═O-based compounds or metal carbonates (532 eV), and C−O-based compounds (533.1 eV). C−O and C═O bonds correspond to the adventitious contamination on the surface. The presence of metal carbonates is due to the incorporation of carbonyl and carboxyl groups into Al-A coating during PEO surface treatment. We observe a Na auger peak (~535 eV) in the deconvoluted O 1s spectrum. Al 2p spectral deconvolution (Figure 7c) resulted in two peaks—one at 74.6 eV indicating the presence of Al−O−Si bonded compounds and the other at 76.2 eV indicating the presence of alumina in the coatings. Si 2p peaks (Figure 7d) indicate the presence of organic silicon (101.9 eV) and silica (103.3 eV) in Al-A coatings.

Figure 8 illustrates the XPS core-level spectra for aluminum alloys treated in aminophenol-modified PEO electrolytes. The C 1s spectrum (Figure 8a) exhibited four deconvoluted speaks. The C−C peak at 284.8 eV and the C−O−C peak at 286.6 eV correspond to the adventitious contamination accumulated on the surface. We attribute the N 1s peak at 400.5 eV to overlapping signatures for $C-NH_2$ and silicon (Figure 8b). The O 1s spectra (Figure 8c) and Al 2p (Figure 8d) spectra are similar for Al-A and Al-B coatings. The Si 2p spectrum (Figure 8e) resolved into three peaks—at 102.7 eV corresponding to aluminosilicate, at 103.7 eV corresponding to organic silicon, and at 104.6 eV corresponding to silica.

The analysis of XRD patterns and XPS spectra for Mg-A, Mg-B, Al-A, and Al-B coatings indicates that the oxide content in the coatings is due to the PEO treatment of the alloys. The decomposition of PEO electrolytes during treatment incorporates metal silicates and carbonates into the coatings. The addition of nitrogen-containing compounds to the electrolytic bath is responsible for the nitride content observed in Mg-B and the silicon oxynitride content in Mg-B and Al-B coatings. Localized elevated temperatures (>3000 °C) obtained during the arc discharge processes could contribute to the formation of nitrides in the coatings.

Mechanical Behavior. Nanoindentation tests, performed on the coating cross sections, evaluated the mechanical behavior of Mg-A, Mg-B, Al-A, and Al-B. The PEO process reported in this paper improved the coatings' hardness by at least 7 times for Mg alloys and by at least 3 times for Al alloys. Untreated AZ80 alloy exhibits a nanohardness of 1.06 GPa. Mg-A coatings exhibit 7.66 GPa, and Mg-B coatings exhibit 8.58 GPa. Untreated Al6061 alloy exhibits 1.81 GPa. Al-A coatings exhibit 5.73 GPa and Al-B coatings exhibit 7.03 GPa. The incorporation of nitrides and oxynitrides into the coating composition improved the hardness of Mg-B by 12% and Al-B by 22%. We attribute the higher deviation in Al-B results to the irregularities in the coating−substrate interfacial layer and the intermittently formed secondary top layer.

Corrosion Behavior. We extracted the corrosion potentials of Mg-A, Mg-B, Al-A, and Al-B coatings from the Tafel plots in Figure 9. Table 1 provides the corrosion potentials and

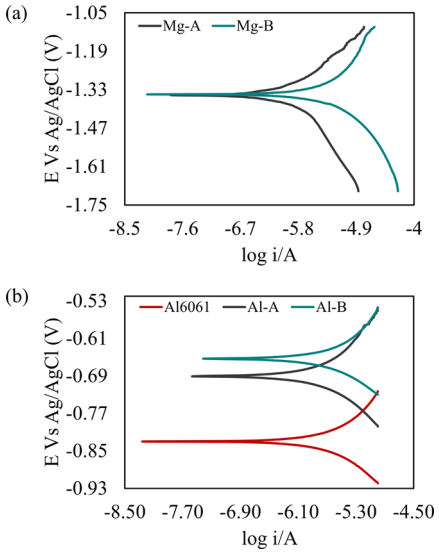

Figure 9. Tafel plots for (a) Mg-A and Mg-B coatings formed on AZ80 alloys and (b) Al-A and Al-B coatings formed on Al6061 alloys by PEO surface treatment without and with aminophenol in the bath chemistry.

Table 1. Corrosion Potential and Current Densities Extracted from Tafel Plots in Figure 9 for PEO-Treated Mg and Al Alloys[a]

	untreated AZ80 alloy	Mg-A	Mg-B
E_{corr} (mV)	−1507[37,38]	−1349.5	−1350.1
i_{corr} (× 10^{-7} A/cm^2)	27.72[37]	8.06	29.49
	untreated Al6061 alloy	Al-A	Al-B
E_{corr} (mV)	−829.9	−689.4	−655.4
i_{corr} (× 10^{-6} A/cm^2)	2.17	1.74	1.99

[a]The data for untreated Mg and Al alloys are available for comparison.

associated current densities. We compared the corrosion performance of Al-A and Al-B with the performance of untreated Al alloys. We obtained the corrosion potentials for untreated Mg alloys from Naik et al. The data extracted from Figure 9a show that the corrosion potentials for Mg-A and Mg-B are similar but the corrosion current for Mg-B is higher. A lower corrosion current implies a lower corrosion rate of Mg-A compared to Mg-B. Our hypothesis: this is due to the higher porosity and the lower thickness of the Mg-B coatings. Figure 9b illustrates the higher corrosion resistance exhibited by Al-A and Al-B compared to untreated Al6061 alloys. The absence of a surface layer in Al-B coatings could contribute to their slightly reduced corrosion resistance. Ma et al. and Shanaghi et al. suggest that nitridation of coatings on Mg and Al alloys has a positive influence on their corrosion resistance.[33,36] Thus, we attribute the slightly reduced corrosion resistance of Mg-B and Al-B alloys to their physical characteristics.

Figure 10 demonstrates the impedance behavior of PEO-treated aluminum alloys vs the untreated substrates. We modeled the electrochemical impedance spectroscopic (EIS)

https://doi.org/10.1021/acsomega.1c06442
ACS Omega 2022, 7, 8570−8580

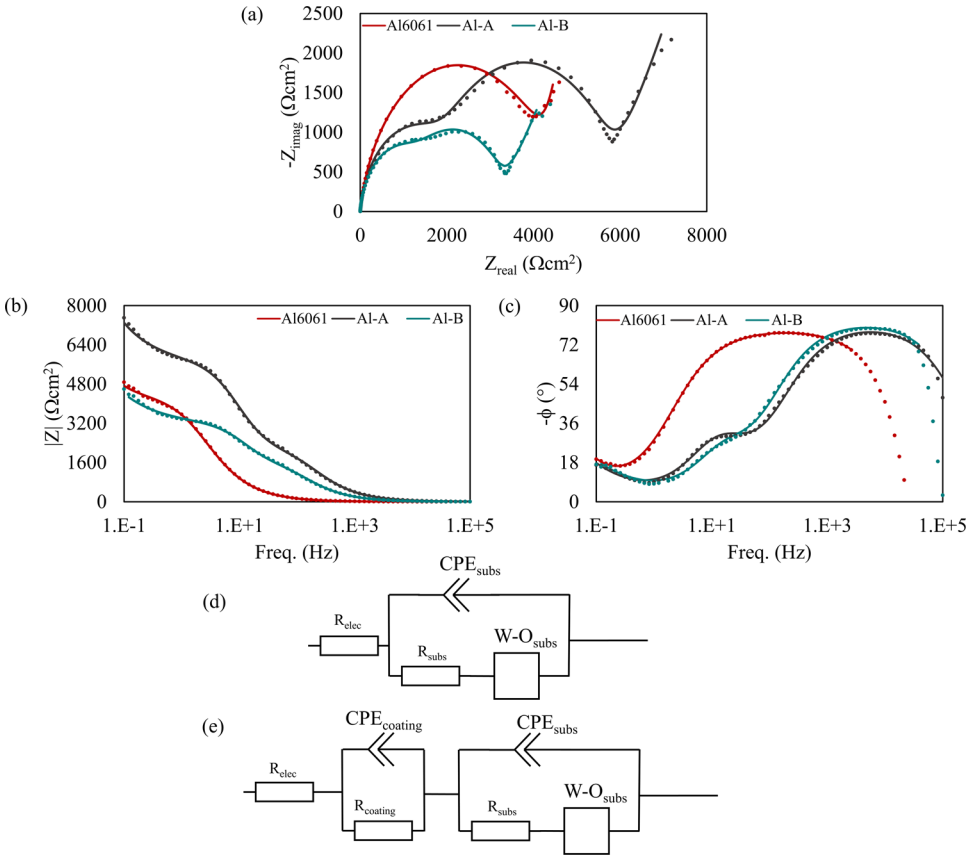

Figure 10. Electrochemical impedance spectroscopy of Al-A and Al-B coatings in comparison with EIS results for bare Al6061 substrate. (a) Nyquist plots; (b, c) Bode plots for Al6061, Al-A, and Al-B; (d) EEC for untreated Al6061 substrate; and (e) EEC modeled for Al-A and Al-B.

response of untreated and PEO-treated substrates using the equivalent electrical circuits (EECs) in Figure 10d and Figure 10e. R_{subs}, $R_{coating}$, and R_{elec} represent the substrate, coating, and electrolyte resistances, respectively. Q represents the admittances of constant phase elements for substrates (CPE_{subs}) and coatings ($CPE_{coating}$). $Z_{Warburg}$ represents the Warburg impedance owing to the diffusion of chemical reactants in the solution. $R_{coating}$ encompasses the resistances of coatings (Al-A/Al-B), pores, and defects and is in parallel with $CPE_{coating}$. We calculated the capacitance of the coatings according to eq 1.

$$C_{coating} = (CPE_{coating} \times R_{coating})^{1/n}/R_{coating} \quad (1)$$

R_{subs} is in series with the Warburg element and parallel with CPE_{subs}. The dotted lines in Nyquist plots (Figure 10a) and Bode plots (Figure 10b,c) represent the impedance response, and the solid lines represent the fitted data. Table 2 lists the respective resistance values. EIS modeling shows that the polarization resistance of Al-A coating is higher than that of Al-B. The capacitance of Al-A is lower than that of Al-B. The results suggest that currently the nitridation of coatings is likely to be detrimental to corrosion behavior. The higher porosity of Al-B coatings potentially contributes to the increased capacitance observed in the coatings. The reduction in $Z_{Warburg}$ also suggests that higher porosity lowers the resistance of the coatings to diffusion of chemical reactants from the solution to the substrate.

Table 2. Fitting Parameters of EIS EECs Obtained for Untreated Al6061, Al-A, and Al-B Surfaces

element	bare Al-6061	Al-A	Al-B
R_{elec} (Ω/cm^{-2})	1.324	3.132	1.428
$R_{coating}$ (Ω/cm^{-2})		1911	1374
$CPE_{coating}$ ($mS/s^n \cdot cm^2$)		0.95	1.71
$n_{coating}$		0.91	0.92
$C_{coating}$ (mF)		1.01	1.84
$R_{substrate}$ (Ω/cm^{-2})	4399	3690	1845
$CPE_{substrate}$ ($\mu S/s^n \cdot cm^2$)	25.22	6.86	9.88
diffusion (ms)	0.4	158.5	3.5
$Z_{Warburg}$ (Ω/cm^{-2})	1.23	545.4	42.59
$n_{Warburg}$	0.42	0.33	0.30

CONCLUSIONS

In conclusion, we have demonstrated that voltages as low as 150 V can reliably produce thick, adherent, and corrosion-resistant coatings on Mg and Al alloys. The coatings exhibit crystalline properties and are composed of metal oxides, silicates, and oxynitrides (in cases where we used amino-phenol-containing electrolyte for surface treatments). Low-energy PEO surface modification can form coatings with enhanced mechanical properties. Mg-A and Al-A coatings exhibit good corrosion resistance behavior. Nitridation of the coatings has a positive influence on their mechanical properties, which are desirable for automotive and semiconductor industry applications. Cirrus Materials Science is currently exploring the use of AC-based PEO treatment to

https://doi.org/10.1021/acsomega.1c06442
ACS Omega 2022, 7, 8570−8580

potentially improve the corrosion resistance of nitride/oxynitride-containing coatings.

MATERIALS AND METHODS

Substrate Preparation and Pretreatment. The current study used magnesium AZ80 alloys and aluminum Al6061 alloys. Prior to PEO processing, the sample surfaces were prepared by mechanically roughening the substrate using emery paper followed by cleaning in a commercially available 80 °C alkaline bath, for 15 min. The pretreatment process ensured the removal of organic contamination from machined substrates. The bath comprises 20 g/L $NaCO_3$, 20 g/L Na_2PO_4, 20 g/L Na_2SiO_3, and 3 g/L OP-10 surfactant. Finally, we used DI water to rinse the substrate. We designed the cleaning process to prevent any buildup of the native oxide layer on the substrate.

PEO Process. We treated two sets each of Mg and Al alloys in a 25 °C PEO bath comprising 70 g/L NaOH, 60 g/L Na_2SiO_3, 10g/L $Na_3C_6H_5O_7$, 6 mL/L H_2O_2, and 0.05 mmol/L sodium dodecyl sulfate (SDS). We prepared two samples sets, "A" and "B", and we added 4.9 mL/L aminophenol to the electrolyte for sample set "B". Alkaline bath chemistry modified with H_2O_2 ensured the generation of oxide coatings on metal surfaces. We used a silicate compound to incorporate silicate content into the coating and enhance the conductivity of the bath. Citrate compounds aided in the uniform distribution of surface arc generation. We used SDS to moderate the physical properties of PEO bath to enhance the removal of gas bubbles generated during processing. We conducted the treatment process for 15 minutes using a stainless-steel counter electrode. A variable-voltage DC power system supplied a constant current of 1 A/dm^2 for Mg and 4 A/dm^2 for Al resulting in an average processing voltage of <160 V.

Morphological Characterization. We used an FEI XL30 SEM equipped with a 30 kV field emission gun to analyze the surface morphologies and composition of the PEO-treated light metal alloys. Prior to imaging, we sputtered the samples with Pt using a Quorum Tech Q150T turbomolecular pumped coater to improve their electron conductivity for SEM imaging.

X-ray Diffraction (XRD). We used a Rigaku XtaLAB Synergy-s single-crystal X-ray diffractometer equipped with a Cu Kα source (λ = 1.54184 Å, 2θ = 20−80°, 0.02° step size) to collect phase and composition data on the oxidized sample surfaces. We analyzed the XRD patterns using the Materials Explorer application on Materials Project open database.[39]

X-ray Photoelectron Spectroscopy (XPS). We employed a Kratos AXIS DLD X-ray photoelectron spectrometer with a hemispherical electron energy analyzer for analyzing the oxide surfaces on Mg and Al alloys. We obtained the spectra using monochromatic Al K_a X-rays (1486 eV) operated at 150 W and maintained the analysis chamber at 1×10^{-9} Torr for data collection. We used survey scans from −5 to 1350 eV (160 eV pass energy) to determine the material composition. We collected core-level data (20 eV pass energy) for C, O, and Si from all of the samples, for N from the samples treated in electrolytic bath modified with nitrogen-containing compounds, and for Mg and Al from the respective alloys. We analyzed the data using Casa XPS 2.3.14 after aligning the C 1s peak at 284.8 eV. Thermo Scientific XPS database was used to analyze the deconvoluted spectral peaks.[40]

Mechanical Behavior. We analyzed the mechanical behavior of the ceramic oxide coatings using a Hysitron TI 950 tribometer equipped with a Berkovich tip. We mounted PEO-treated magnesium and aluminum sample cross sections in epoxy for the nanoindentation tests to eliminate any interference from the underlying substrate. We applied a maximum load of 1000 mN for 2 s with 5 s preloading and unloading times. Nanoindentation tests on nonoxidized control substrates aided in evaluating the mechanical enhancement provided by the ceramic coating.

Corrosion Resistance. To evaluate the electrochemical performance of the PEO-treated coatings, we used a CH Instruments three-cell electrochemical workstation equipped with a Metek designed K0235 flat cell kit. We immersed the samples in 3.5 wt % NaCl solution for 30 min, prior to testing. The tests employed a Ag/AgCl reference electrode and a Pt counter electrode. We used a freshly prepared 3.5 wt % NaCl solution for Tafel and EIS tests. We scanned the open-circuit potential (OCP) of the coatings from −0.3 to 0.3 V for 5 min for Tafel tests. We also measured the EIS of the ceramic coatings between 0.1 Hz and 10 kHz frequencies with a perturbation amplitude of 10 mV.

AUTHOR INFORMATION

Corresponding Author

Rukmini Gorthy − *Cirrus Materials Science Ltd., Auckland 0627, New Zealand;* orcid.org/0000-0003-1886-3739; Phone: +64 27 446 0695; Email: minni.gorthy@cirrusmaterials.com

Authors

Fengyan Hou − *Cirrus Materials Science Ltd., Auckland 0627, New Zealand*

Ian Mardon − *Cirrus Materials Science Ltd., Auckland 0627, New Zealand*

Da Tang − *Cirrus Materials Science Ltd., Auckland 0627, New Zealand*

Chris Goode − *Cirrus Materials Science Ltd., Auckland 0627, New Zealand*

Complete contact information is available at: https://pubs.acs.org/10.1021/acsomega.1c06442

Author Contributions

All authors contributed to the manuscript drafting and have given their approval to the final version of the manuscript.

Notes

The authors declare no competing financial interest.

ACKNOWLEDGMENTS

The authors thank Catherine Hobbis and Colin Doyle of Research Centre for Surface and Materials Science at The University of Auckland (UoA). They also thank Tianping Zhu for assisting with potentiodynamic testing of the coatings. They are grateful to Prof. Wei Gao for providing them with access to the characterization facilities at UoA. Callaghan Innovation partially funded this research project

REFERENCES

(1) Atak, A.; Şik, A. *Investigation of Mechanical Properties and Fatigue of Friction Stir Spot Welded Light Metals*; Springer International Publishing, Cham: Cham, 2019; 343−349.

(2) Wu, G. S.; Shanaghi, A.; Zhao, Y.; Zhang, X. M.; Xu, R. Z.; Wu, Z. W.; Li, G. Y.; Chu, P. K. The effect of interlayer on corrosion resistance of ceramic coating/Mg alloy substrate in simulated physiological environment. *Surf. Coat. Technol.* **2012**, *206*, 4892−4898.

(3) Liu, J. B.; Xiong, J.; Zhou, L.; Guo, Z. X.; Wen, H. T.; You, Q. B.; Li, X. R.; Liu, J.; Zhao, W. Properties of TiN-Al2O3-TiCN-TiN, TiAlN, and DLC-coated Ti(C,N)-based cermets and their wear behaviors during dry cutting of 7075 aluminum alloys. *Int. J. Appl. Ceram. Technol.* **2021**, *18*, 792−802.
(4) Noder, J.; George, R.; Butcher, C.; Worswick, M. J. Friction characterization and application to warm forming of a high strength 7000-series aluminum sheet. *J. Mater. Process. Technol.* **2021**, *293*, No. 117066.
(5) Ishizaki, T.; Hieda, J.; Saito, N.; Saito, N.; Takai, O. Corrosion resistance and chemical stability of super-hydrophobic film deposited on magnesium alloy AZ31 by microwave plasma-enhanced chemical vapor deposition. *Electrochim. Acta* **2010**, *55*, 7094−7101.
(6) Gadow, R.; Scherer, D. Composite coatings with dry lubrication ability on light metal substrates. *Surf. Coat. Technol.* **2002**, *151*−*152*, 471−477.
(7) Shadanbaz, S.; Dias, G. J. Calcium phosphate coatings on magnesium alloys for biomedical applications: A review. *Acta Biomater.* **2012**, *8*, 20−30.
(8) Wang, D.; Bierwagen, G. R. Sol-gel coatings on metals for corrosion protection. *Prog. Org. Coat.* **2009**, *64*, 327−338.
(9) Vazirinasab, E.; Jafari, R.; Momen, G. Application of superhydrophobic coatings as a corrosion barrier: A review. *Surf. Coat. Technol.* **2018**, *341*, 40−56.
(10) Luan, B. L.; Yang, D.; Liu, X. Y.; Song, G. L. 15 - Corrosion Protection of Magnesium (Mg) Alloys using Conversion and Electrophoretic Coatings. In *Corrosion of Magnesium Alloys*; Song, G.-l., Ed.; Woodhead Publishing, 2011; Vol. 7, pp 541−564.
(11) Becker, M. Chromate-free chemical conversion coatings for aluminum alloys. *Corros. Rev.* **2019**, *37*, 321−342.
(12) Zhou, P.; Yu, B. X.; Hou, Y. J.; Duan, G. Q.; Yang, L. X.; Zhang, B.; Zhang, T.; Wang, F. H. Revisiting the cracking of chemical conversion coating on magnesium alloys. *Corros. Sci.* **2021**, *178*, No. 109069.
(13) Cao, F.; Song, G.-L.; Atrens, A. Corrosion and passivation of magnesium alloys. *Corros. Sci.* **2016**, *111*, 835−845.
(14) Gu, C. D.; Lian, J. S.; He, J. G.; Jiang, Z. H.; Jiang, Q. High corrosion-resistance nanocrystalline Ni coating on AZ91D magnesium alloy. *Surf. Coat. Technol.* **2006**, *200*, 5413−5418.
(15) Abbott, A. P.; Frisch, G.; Ryder, K. S. Electroplating Using Ionic Liquids. *Annu. Rev. Mater. Res.* **2013**, *43*, 335−358.
(16) Walsh, F. C.; Low, C. T. J.; Wood, R. J. K.; Stevens, K. T.; Archer, J.; Poeton, A. R.; Ryder, A. Plasma electrolytic oxidation (PEO) for production of anodised coatings on lightweight metal (Al, Mg, Ti) alloys. *Trans. IMF* **2009**, *87*, 122−135.
(17) Malyshev, V. N.; Markov, G. A.; Fedorov, V. A.; Petrosyants, A. A.; Terleeva, O. P. Features of the structure and properties of coatings applied by the method of microarc oxidation. *Chem. Pet. Eng.* **1984**, *20*, 41−43.
(18) Markov, G. A.; Mironova, M. K.; Potapova, O. G.; Tatarchuk, V. V. STRUCTURE OF ANODIC FILMS FORMED BY THE MICROARC OXIDATION OF ALUMINUM. *Inorg. Mater.* **1983**, *19*, 1000−1004.
(19) Zhang, Y.; Xu, Y.; Miao, C.; Tu, X.; Yu, J.; Li, J. Effect of Tungsten Carbide Particles on the Characteristics of PEO Coatings Formed on AZ31B Magnesium Alloy in Alkaline Electrolyte. *Int. J. Electrochem. Sci.* **2018**, *13*, 7923−7929.
(20) Pardo, A.; Casajus, P.; Mohedano, M.; Coy, A. E.; Viejo, F.; Torres, B.; Matykina, E. Corrosion protection of Mg/Al alloys by thermal sprayed aluminium coatings. *Appl. Surf. Sci.* **2009**, *255*, 6968−6977.
(21) Matykina, E.; Arrabal, R.; Mohedano, M.; Mingo, B.; Gonzalez, J.; Pardo, A.; Merino, M. C. Recent advances in energy efficient PEO processing of aluminium alloys. *Trans. Nonferrous Met. Soc. China* **2017**, *27*, 1439−1454.
(22) Pezzato, L.; Brunelli, K.; Napolitani, E.; Magrini, M.; Dabala, M. Surface properties of AZ91 magnesium alloy after PEO treatment using molybdate salts and low current densities. *Appl. Surf. Sci.* **2015**, *357*, 1031−1039.
(23) Lee, K. M.; Ko, Y. G.; Shin, D. H. Incorporation of carbon nanotubes into micro-coatings film formed on aluminum alloy via plasma electrolytic oxidation. *Mater. Lett.* **2011**, *65*, 2269−2273.
(24) Mashtalyar, D. V.; Sinebryukhov, S. L.; Imshinetskiy, I. M.; Gnedenkov, A. S.; Nadaraia, K. V.; Ustinov, A. Y.; Gnedenkov, S. V. Hard wearproof PEO-coatings formed on Mg alloy using TiN nanoparticles. *Appl. Surf. Sci.* **2020**, *503*, No. 144062.
(25) Dehnavi, V.; Luan, B. L.; Shoesmith, D. W.; Liu, X. Y.; Rohani, S. Effect of duty cycle and applied current frequency on plasma electrolytic oxidation (PEO) coating growth behavior. *Surf. Coat. Technol.* **2013**, *226*, 100−107.
(26) Darband, B. G.; Aliofkhazraei, M.; Hamghalam, P.; Valizade, N. Plasma electrolytic oxidation of magnesium and its alloys: Mechanism, properties and applications. *J. Magnesium Alloys* **2017**, *5*, 74−132.
(27) Hoche, H.; Scheerer, H.; Probst, D.; Broszeit, E.; Berger, C. Development of a plasma surface treatment for magnesium alloys to ensure sufficient wear and corrosion resistance. *Surf. Coat. Technol.* **2003**, *174*−*175*, 1018−1023.
(28) Cai, J. S.; Cao, F. H.; Chang, L. R.; Zheng, J. J.; Zhang, J. Q.; Cao, C. A. The preparation and corrosion behaviors of MAO coating on AZ91D with rare earth conversion precursor film. *Appl. Surf. Sci.* **2011**, *257*, 3804−3811.
(29) Dong, K. H.; Song, Y. W.; Shan, D. Y.; Han, E. H. Formation mechanism of a self-sealing pore micro-arc oxidation film on AM60 magnesium alloy. *Surf. Coat. Technol.* **2015**, *266*, 188−196.
(30) Zhang, Y.; Wu, Y. K.; Chen, D.; Wang, R. Q.; Li, D. L.; Guo, C. H.; Jiang, G. R.; Shen, D. J.; Yu, S. X.; Nash, P. Micro-structures and growth mechanisms of plasma electrolytic oxidation coatings on aluminium at different current densities. *Surf. Coat. Technol.* **2017**, *321*, 236−246.
(31) Clyne, T. W.; Troughton, S. C. A review of recent work on discharge characteristics during plasma electrolytic oxidation of various metals. *Int. Mater. Rev.* **2019**, *64*, 127−162.
(32) Sikdar, S.; Menezes, P. V.; Maccione, R.; Jacob, T.; Menezes, P. L. Plasma Electrolytic Oxidation (PEO) Process-Processing, Properties, and Applications. *Nanomaterials* **2021**, *11*, 1375.
(33) Shanaghi, A.; Mehrjou, B.; Chu, P. K. Enhanced corrosion resistance and reduced cytotoxicity of the AZ91 Mg alloy by plasma nitriding and a hierarchical structure composed of ciprofloxacin-loaded polymeric multilayers and calcium phosphate coating. *J. Biomed. Mater. Res. Part A* **2021**, *109*, 2657−2672.
(34) Khairallah, F.; Glisenti, A. Synthesis, characterization and reactivity study of nanoscale magnesium oxide. *J. Mol. Catal. A: Chem.* **2007**, *274*, 137−147.
(35) Qin, Y.; Wu, M.; Yang, G.; Yang, Y.; Zhao, L. Tribological Performance of Magnesium Silicate Hydroxide/Ni Composite as an Oil-Based Additive for Steel−Steel Contact. *Tribol. Lett.* **2021**, *69*, No. 19.
(36) Ma, L. Z.; Huang, J. W.; Fan, X. M.; Li, J. L.; Zhu, H. G.; Xiong, D. S. Properties of thick ceramic composite coatings synthesized on an aluminium alloy by cathodic plasma electrolytic deposition. *Surf. Coat. Technol.* **2018**, *356*, 80−88.
(37) Naik, G. M.; Gote, G. D.; Narendranath, S.; Satheesh Kumar, S. S. The impact of homogenization treatment on microstructure microhardness and corrosion behavior of wrought AZ80 magnesium alloys in 3.5 wt% NaCl solution. *Mater. Res. Express* **2018**, *5*, No. 086513.
(38) Say, W. C.; Chen, C. C.; Hsieh, S.-J. Electrochemical characterization of non-chromate surface treatments on AZ80 magnesium. *Mater. Charact.* **2008**, *59*, 1400−1406.
(39) Jain, A.; Ong, S. P.; Hautier, G.; Chen, W.; Richards, W. D.; Dacek, S.; Cholia, S.; Gunter, D.; Skinner, D.; Ceder, G.; Persson, K. A. Commentary: The Materials Project: A materials genome approach to accelerating materials innovation. *APL Mater.* **2013**, *1*, No. 011002.
(40) ThermoFisherScientific, XPS Simplified/Elements Table, https://xpssimplified.com/periodictable.php.

https://doi.org/10.1021/acsomega.1c06442
ACS Omega 2022, 7, 8570−8580